Low Frequency Fluctuations in a Multimode Semiconductor Laser with Optical Feedback

E. A. Viktorov
Institute for Laser Physics, 199034 St. Petersburg, Russia

Paul Mandel
Optique Nonlinéaire Théorique, Université Libre de Bruxelles, Campus Plaine CP 231, B-1050 Bruxelles, Belgium
(Received 26 January 2000)

We study a multimode semiconductor laser subject to a moderate optical feedback. The steady state is destabilized by either a simple Hopf bifurcation leading to in phase dynamics or by a degenerate Hopf bifurcation leading to antiphase dynamics. The degenerate bifurcation is also a source of multiple coexisting attractors. We show that a simple interpretation of the low frequency fluctuations in the multimode regime is provided by a chaotic itinerancy among the many coexisting unstable attractors produced by the degenerate Hopf bifurcation.

PACS numbers: 42.55.Px, 42.60.Mi

Semiconductor lasers are prone to instabilities when subjected to an optical feedback. In most applications, the optical feedback is difficult to avoid and may lead to a loss of useful properties. An example is the occurrence of low frequency fluctuations (LFF) which are observed near the lasing threshold. This phenomenon is characterized by intensity dropouts with an average time between dropouts much longer than either relaxation oscillation periods or mode beating characteristic times. The LFF regime has been observed experimentally first using a bandwidth limited detector [1], and recently confirmed by means of high bandwidth streak camera experiments [2]. The modelization of this behavior is difficult because the characteristic time scales involved in the laser dynamics are too short to allow a direct detection by electronic means. Noise-driven models have been proposed to describe the LFF effect [3]. A deterministic approach, based on the single mode Lang-Kobayashi (LK) equations [4], was proposed in [5] to explain the LFF as a chaotic itinerancy with a drift [6]. Recently, there have been strong indications that the LFF need not be irregular: the laser can produce a train of equally spaced pulses [7]. Most studies of the LFF have been limited so far to single mode models. However, recent experiments have demonstrated the growing importance of a multimode operation in the LFF regime [8]. A key result for the modelization is the experimental evidence that the dynamics of the modal intensities can be antiphased: the characteristic nonoptical frequencies are still controlled by the external cavity round-trip time, but the oscillation phases differ from mode to mode [9]. A phenomenological multimode model has recently been proposed in [10]. It describes a multimode operation, but in the time-dependent regime the modes are always in phase. The goal of this Letter is to introduce a multimode extension of the LK model which accounts for the possibility of antiphase dynamics. We achieve this goal by taking into account the grating associated with a Fabry-Perot configuration. This model is able to describe both the in phase and the out of phase dynamics which are observed experimentally. It predicts two possible instabilities for the steady states: a standard self-pulsing instability where all modes are in phase, and a new $(N-1)$-degenerate Hopf bifurcation where N is the number of lasing modes. Depending on the experimental conditions, either of these two bifurcations can be the first to destabilize the steady state. The degenerate Hopf bifurcation generates coexisting periodic and quasiperiodic attractors [11]. The main consequence of our analysis is that in the multimode regime the LFF can be interpreted as a chaotic itinerancy among the coexisting unstable attractors originating from the degenerate Hopf bifurcation.

Laser rate equations can be derived for the modal intensities $E_m(t) \propto \int E(x,t)\phi_m(x)\,dx$ coupled either to both the population gratings $H_m(t) \propto \int N(x,t)[1-\phi_m^2(x)]\,dx$ and the population average $H(t) \propto \int N(x,t)\,dx$ or to the nonlinear gains $N_m(t) \propto \int N(x,t)\phi_m^2(x)\,dx$ where $\phi_m(x) = 2^{1/2}\sin(q_m x)$ is a lasing cavity eigenmode. The usual description of lasers [12,13] based on rate equations couples the $2N+1$ variables $\{E_m, H_m, H\}$. Multimode intracavity second harmonic generation lasers [14] are described by $2N$ Baer rate equations which couple the variables $\{E_m, N_m\}$. Since the single mode semiconductor laser rate equations couple the variables $\{E_m, N_m\}$ for one given m, it is easy to extend them to the multimode regime in analogy with the Baer multimode equations. Introducing a modal feedback as in the LK formulation leads to

$$\frac{dE_m}{dt} = \frac{1}{2}(1+i\alpha)[N_m - \gamma_{pm}]E_m + k_m E_m(t-\tau)e^{-i\Omega_m\tau},$$

$$\frac{dN_m}{dt} = J - \frac{N_m}{\tau_s} - N_m\sum_n^N \beta_{nm}|E_n|^2,$$

where $\beta_{mm} = 1$. The mode index m varies from 1 to N, the number of lasing modes. In the field equations, γ_{pm}

denotes the modal field losses and α is the linewidth enhancement factor. The feedback is characterized by the attenuation coefficients k_m, $E_m(t-\tau)$ is the modal field delayed by one round-trip time τ, and $-i\Omega_m\tau$ is the phase mismatch after one round-trip. In the nonlinear gain equations, J is the pumping current and τ_s is the carrier lifetime. The cross-saturation parameters $0 < \beta_{nm} < 1$ measure the population inversion grating.

To simplify the analysis, γ_{pm}, k_m, and β_{nm} are assumed mode independent: $\gamma_{pm} \equiv \gamma_p$, $k_m \equiv k$, and $\beta_{nm} = \beta$ with $m \neq n$. The gain at threshold is $N_{th} = \gamma_p$ and we introduce the deviation n_m from this threshold value $N_m = \gamma_p + n_m$. The normalized multimode equations describing the semiconductor laser with optical feedback become

$$\frac{dA_m}{d(\gamma_p t)} = (1 + i\alpha)F_m A_m + \eta A_m(t-\tau)e^{-i\Omega_m\tau}, \quad (1)$$

$$T\frac{dF_m}{d(\gamma_p t)} = P - F_m - (1 + 2F_m)\sum_n^N \beta_{nm}|A_n|^2, \quad (2)$$

where

$$A_m = \sqrt{\tau_s/2}\,E_m, \qquad F_m = n_m/2\gamma_p,$$
$$P = (J - J_{th})/2J_{th},$$

with $J_{th} = \gamma_p/\tau_s$, $T = \tau_s\gamma_p$, and $\eta = k/\gamma_p$.

The key feature in Eqs. (1) and (2) is the introduction of the carrier moments F_m which are proportional to the grating created by the field. Neglecting these gratings, i.e., $F_m \simeq F_0$, Eqs. (1) and (2) reduce to the $N+1$ equations of [10]. It is commonly assumed that the carrier grating does not contribute to the semiconductor laser dynamics because it should be washed out by diffusion. However, it is difficult to argue along this line since there are no direct measurements of the relevant parameters with sufficient accuracy to dismiss or support the role of carrier grating. What is clear is that diffusion tends to reduce the number of oscillating modes [15]. The only possibility of finding antiphase dynamics with the $N+1$ equations is in the transient evolution, starting with properly selected initial conditions.

Equations (1) and (2) extend the LK model to the multimode regime. The delay term leads to the possible existence of multiple steady states in the single mode regime [16]. A multimode extension naturally preserves this feature. However, since we have assumed that all physical parameters are mode independent, we also assume that all modes are in the same steady state. This property is supported by the numerical simulations. This steady state solution of Eqs. (1) and (2) is of the form $A_m(t) = A\exp[i\varphi(t)]$ and $F_m = F$. The solution is stationary because its modal intensities are constant.

The linear stability of this degenerate solution indicates that there are two routes for the destabilization of the steady state. They are related to the occurrence of two possible Hopf bifurcations with very different properties. One Hopf bifurcation is nondegenerate and corresponds to undamped oscillations associated with the relaxation oscillation frequency Ω_R. This frequency is close to the single mode relaxation oscillation frequency. A property of the periodic solutions which emerges at that point is $A_m(t) = A(t)$ and $F_m(t) = F(t)$: all modes oscillate in phase. The in phased solutions of Eqs. (1) and (2) are identical to the solutions of the multimode equations derived in [10]. The novelty brought in by the introduction of nonlinear modal gains is the existence of a second Hopf bifurcation associated with the frequency $\Omega_L < \Omega_R$. Its main characteristic is to be $(N-1)$ degenerate: there are $N-1$ eigenvectors of the Jacobian matrix with the same eigenvalue. These eigenvectors correspond to identical field intensities but different phases. The simplest of these solutions is $A_m(t) = [A_m + a\exp(2\pi inm/N)]\exp[i\varphi(t)]$ where $n = 1, 2, \ldots, N-1$. Similar problems displaying a degenerate Hopf bifurcation have recently been investigated analytically for multimode solid-state lasers [11]. In that work, we have analyzed the mechanism by which the degenerate Hopf bifurcation generates quasiperiodic rather than periodic stable solutions. The situation is similar for Eqs. (1) and (2), though the delay makes the analysis much heavier. Therefore, we only display numerical results to illustrate the properties of the model.

To fix orders of magnitude, the two relaxation oscillation frequencies have been determined numerically from the response of the steady state to small amplitude noise for $P = 10^{-3}$, $T = 10^3$, $\gamma_p = 1$ THz, $\alpha = 5$, $\beta = 0.666$, $\eta = 10^{-4}$, and $\Omega_m = 2m\pi/\tau$ with m integer. For $\tau = 1.2$ ns, we have $\Omega_L \simeq 190$ MHz, $\Omega_R \simeq 370$ MHz, and the Hopf bifurcation occurs at $\eta_H = 6 \times 10^{-4}$.

Let us begin by considering the influence of the delay on the solutions of Eqs. (1) and (2). This is analyzed in Fig. 1 where we display the total output for $N = 3$ and delays ranging from 1.2 to 9 ns. In order to match the experimental results, we have averaged the time series over 1 GHz, corresponding to the bandwidth of the usual experimental recorders. The total output clearly shows the presence of the low frequency fluctuations. The period of fluctuations depends on the delay, and Fig. 1 indicates a nonmonotonic dependence.

The dynamics of the LFF regime displayed for the shortest external cavity (Fig. 1a) is in phase, as can be verified by checking the modal field amplitudes, and emerges from the nondegenerate Hopf bifurcation. The scenario leading to Fig. 1a involves only in phased states: as the feedback parameter η increases, the steady state solution loses stability to the stable periodic state via a Hopf bifurcation, followed by a secondary Hopf bifurcation which leads to a quasiperiodic state which eventually becomes chaotic as shown in Fig. 1a.

The dynamics in Fig. 1d is much slower. In this case, the low frequency fluctuations are associated with the degenerate Hopf bifurcation at Ω_L. These solutions are difficult to interpret. We shall therefore first discuss periodic and quasiperiodic solutions (displayed in Fig. 2) leading to

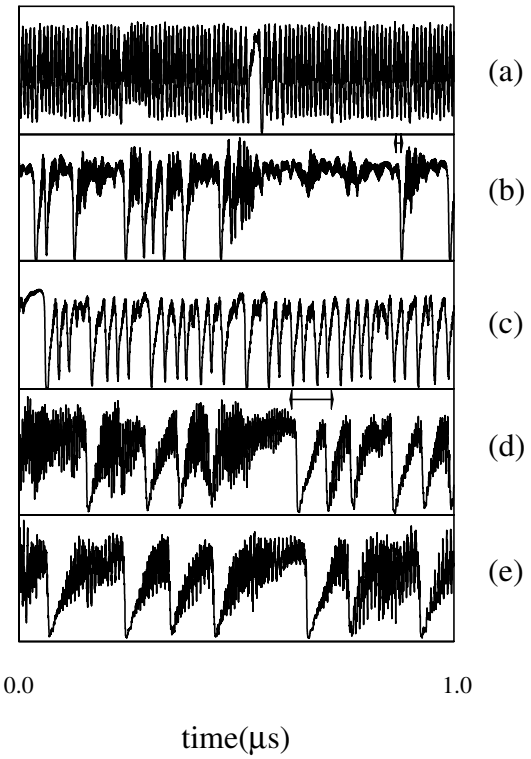

FIG. 1. Total output from Eqs. (1) and (2) featuring LFF for $N = 3$ averaged during 1 GHz. The fixed parameters are $P = 10^{-3}$, $T = 10^3$, $\gamma_p = 1$ THz, $\alpha = 5$, $\beta = 0.666$, $\eta = 7.5 \times 10^{-3}$, and $\Omega_m = 2n\pi/\tau$ with n integer. Delays are (a) $\tau = 1.2$ ns, (b) $\tau = 1.5$ ns, (c) $\tau = 2$ ns, (d) $\tau = 6$ ns, and (e) $\tau = 9$ ns.

the chaotic regime and then the chaotic modal intensities (displayed in Fig. 3) corresponding to the total intensity shown in Fig. 1d.

Figure 2a shows the periodic solution at $\eta_H = 1.75 \times 10^{-4}$ emerging from the steady state via the degenerate Hopf bifurcation which takes place at $\eta_H \simeq 1.7 \times 10^{-4}$. It corresponds to a pure periodic antiphase state: all modes are in the same periodic regime but phase shifted by $1/N$ of a period from each other. At a finite distance of this first bifurcation, the solution becomes unstable via a secondary Hopf bifurcation that results in the quasiperiodic state displayed in Figs. 2b–2d. In Figs. 2b–2d the carrier wave has the temporal pattern $\{1, 3, 2\}$ and the envelope modulation has the temporal pattern $\{1, 2, 3\}$, where the numbers indicate the relative phase shift between the modal solutions [11]. By symmetry, the exchange of the pairs $\{1, 3, 2\}$ and $\{1, 2, 3\}$ generates a new solution. Such quasiperiodic solutions can be interpreted simply as a result of interaction between two antiphase periodic states [11]. The main result of this interaction is the formation of a quasiperiodic envelope. The envelope is modulated by a low frequency which depends on the distance from the Hopf bifurcation. The envelope has an asymmetric profile characterized by fast drops followed by a long period of amplitude increase as sketched in Figs. 2b–2d. As the distance from the Hopf bifurcation increases, the system bifurcates from quasiperiodic to chaotic attractors. Thus the

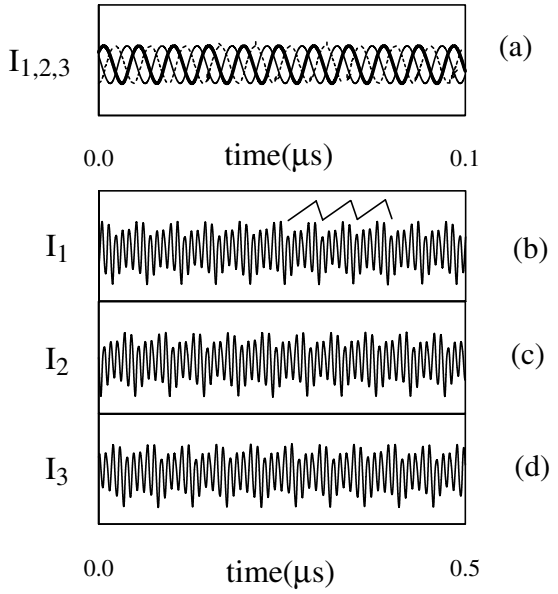

FIG. 2. Modal intensities featuring (a) periodic solution for $\eta = 1.75 \times 10^{-4}$; (b)–(d) quasiperiodic solutions for $\eta = 2 \times 10^{-4}$. Other parameters are as in Fig. 1d. For the quasiperiodic solutions, the carrier wave has the temporal pattern $\{1, 2, 3\}$ and the envelope modulation follows the temporal pattern $\{1, 3, 2\}$. In (b) we have indicated qualitatively the variation of the field envelope to stress the asymmetry between the rise and the fall segments.

LFF are not necessarily chaotic, as the quasiperiodic motion described here could induce a synchronous Sisyphus effect of the type observed experimentally [7]. Note that the degenerate Hopf bifurcation is an instability associated with the low relaxation oscillation frequency Ω_L which is given by $\Omega_L^2 = \Omega_R^2(1 - \beta)/[1 + \beta(N - 1)]$. Since

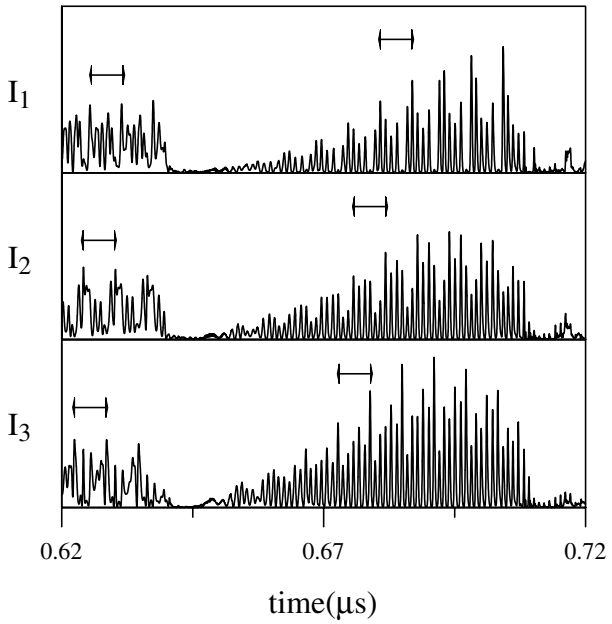

FIG. 3. Modal intensities for the time segment marked in Fig. 1d. The highest peaks are shifted from mode to mode and demonstrate antiphase dynamics. The marked period is the external cavity round-trip time.

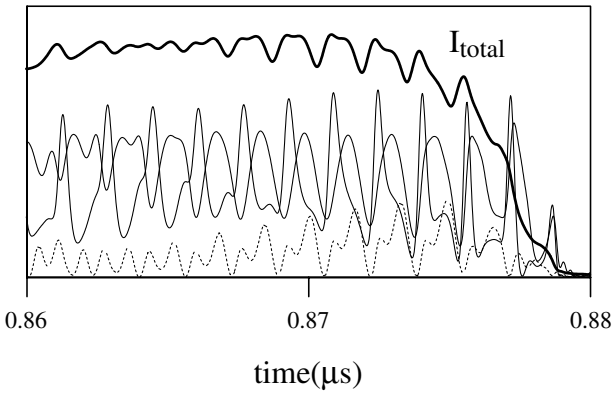

FIG. 4. Modal intensities for the period marked in Fig. 1b. The modal intensities are antiphase and display unstable periodic motion. Despite the switches between different antiphase periodic states, the total output remains nearly constant within the marked period, before the jump to a quasiperiodic state.

$0 \leq \beta \leq 1$, the choice of β does not affect the existence of this Hopf bifurcation, but it will influence the domain of stability of the various solutions beyond the bifurcations.

Now we can compare the periodic antiphase dynamics shown in Figs. 2b–2d and the modal dynamics in the LFF regime of Fig. 1d, which is displayed in Fig. 3 without time averaging. First of all, the period of the envelope in Fig. 3 (indicated by arrows) is nearly the same as for the quasiperiodic antiphase states just after the degenerate Hopf bifurcation in Figs. 2b–2d. The asymmetric profile and the antiphase structure of the motion are also preserved. The left part of Fig. 3 shows unstable periodic modal intensities while the right part of the figure shows unstable quasiperiodic modal intensities. Therefore, we may conclude that the temporal behavior in Fig. 1d is a random itinerancy among the ruins of periodic and quasiperiodic attractors. The antiphase dynamics may lead to a strong reduction of the fluctuations around the unstable steady state between the jumps as shown in Fig. 1b. The large amplitude fluctuations present in the individual modes compensate in the sum intensity.

The temporal patterns of the total output can be very complicated for some values of the delay, but the main features, namely, antiphase fluctuations with low frequency envelopes, persist for the range of delays analyzed here. Figure 1b, for instance, presents at least two time scales associated with the LFF. The LFF drops in Fig. 1 are always associated with jumps from an unstable periodic or quasiperiodic attractor to another unstable quasiperiodic attractor. This is especially visible in Figs. 1d and 1e. The total output varies little between the jumps as a result of the antiphase character of the individual mode temporal behavior. Figure 4 displays the details of the modal behavior for the time segment marked in Fig. 1b. What is shown there is precisely the observation reported in [9]. Namely, as the dropout time approaches, two modes which were in antiphase tend to lock in phase and amplitude while the third mode is in antiphase. Another result reported in the same reference is also easily explained in terms of the multimode model (1) and (2): since the LFF corresponds to jumps between different asymmetric attractors, the rule is that the dominant mode is not the same before and after the jump.

In conclusion, we have proposed a new description of the multimode semiconductor laser with external feedback. We used the experimental evidence to infer the type of multimode equations needed for the laser description. We find that in the multimode regime the LFF can be interpreted as a chaotic itinerancy among the unstable coexisting attractors related to a degenerate Hopf bifurcation. In the domain we have investigated, the periodic attractors and the quasiperiodic attractors differ only by a permutation of the lasing modes.

This research has been supported by the Fonds National de la Recherche Scientifique, the Inter-University Attraction Pole program of the Belgian government, and an INTAS grant.

[1] C. Risch and C. Voumard, J. Appl. Phys. **48**, 2083 (1977).
[2] I. Fischer, G. H. M. van Tartwijk, A. M. Levine, W. Elsasser, E. Gobel, and D. Lenstra, Phys. Rev. Lett. **76**, 220 (1996).
[3] J. Mork, B. Tromborg, and P. L. Christiansen, IEEE J. Quantum Electron. **24**, 123 (1988); A. Hohl, H. J. C. van der Linden, and R. Roy, Opt. Lett. **20**, 2396 (1995).
[4] R. Lang and K. Kobayashi, IEEE J. Quantum Electron. **16**, 347 (1980).
[5] T. Sano, Phys. Rev. A **50**, 2719 (1994); G. H. M. van Tartwijk, A. M. Levine, and D. Lenstra, IEEE J. Sel. Top. Quantum Electron. **1**, 466 (1995).
[6] A. Hohl and A. Gavrielides, Phys. Rev. Lett. **82**, 1148 (1999).
[7] A. Gavrielides, T. C. Newell, V. Kovanis, R. G. Harrison, N. Swanston, Dejin Yu, and Weiping Lu, Phys. Rev. A **60**, 1577 (1999).
[8] G. Huyet, S. Balle, M. Giudici, C. Green, G. Giacomelli, and J. Tredicce, Opt. Commun. **149**, 341 (1998); G. Huyet, S. P. Hegarty, M. Giudici, B. de Bruyn, and J. G. McInerney, Europhys. Lett. **40**, 619 (1997).
[9] G. Vaschenko, M. Giudici, J. J. Rocca, C. S. Menoni, J. Tredicce, and S. Balle, Phys. Rev. Lett. **81**, 5536 (1998).
[10] D. W. Sukow, T. Heil, I. Fischer, A. Gavrielides, A. Hohl-AbiChedid, and W. Elsasser, Phys. Rev. A **60**, 667 (1999).
[11] A. G. Vladimirov, E. A. Viktorov, and P. Mandel, Phys. Rev. E **60**, 1616 (1999).
[12] C. L. Tang, H. Statz, and G. deMars, J. Appl. Phys. **34**, 2289 (1963).
[13] P. Mandel, *Theoretical Problems in Cavity Nonlinear Optics* (Cambridge University Press, Cambridge, England, 1997).
[14] T. Baer, J. Opt. Soc. Am. B **3**, 1175 (1986).
[15] P. A. Khandokhin, I. V. Koryukin, Ya. I. Khanin, and P. Mandel, IEEE J. Quantum Electron. **31**, 647 (1995).
[16] T. Heil, I. Fischer, and W. Elsasser, Phys. Rev. A **60**, 634 (1999).